Equilibrium phase behavior of gyroid-forming diblock polymer thin films \odot

Benjamin R. Magruder 💿 ; Christopher J. Ellison 💿 ; Kevin D. Dorfman 🖼 💿



J. Chem. Phys. 161, 084902 (2024) https://doi.org/10.1063/5.0224767





Articles You May Be Interested In

Following the nucleation pathway from disordered liquid to gyroid mesophase

J. Chem. Phys. (April 2019)

Simulations of the gyroid phase in diblock copolymers with the Gaussian disphere model

J. Chem. Phys. (December 2010)

Simulation of the gyroid phase in off-lattice models of pure diblock copolymer melts

J. Chem. Phys. (September 2006)







Equilibrium phase behavior of gyroid-forming diblock polymer thin films

Cite as: J. Chem. Phys. 161, 084902 (2024); doi: 10.1063/5.0224767

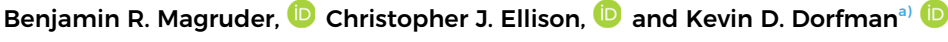
Submitted: 21 June 2024 • Accepted: 5 August 2024 •

Published Online: 22 August 2024











AFFILIATIONS

Department of Chemical Engineering and Materials Science, University of Minnesota - Twin Cities, 421 Washington Avenue SE, Minneapolis, Minnesota 55455, USA

a) Author to whom correspondence should be addressed: dorfman@umn.edu

ABSTRACT

Thin-film confinement of self-assembling block polymers results in materials with myriad potential applications—including membranes and optical devices—and provides design parameters for altering phase behavior that are not available in the bulk, namely, film thickness and preferential wetting. However, most research has been limited to lamella- and cylinder-forming polymers; three-dimensional phases, such as double gyroid (DG), have been observed in thin films, but their phase behavior under confinement is not yet well understood. We use self-consistent field theory to predict the equilibrium morphology of bulk-gyroid-forming AB diblock polymers under thin-film confinement. Phase diagrams reveal that the (211) orientation of DG, often observed in experiments, is stable between nonpreferential boundaries at thicknesses as small as 1.2 times the bulk DG lattice parameter. The (001) orientation is stable between modestly B-preferential boundaries, where B is the majority block, while a different (211)-oriented termination plane is stabilized by strongly B-preferential boundaries, neither of which has been observed experimentally. We then describe two particularly important phenomena for explaining the phase behavior of DG thin films at low film thicknesses. The first is "constructive interference," which arises when distortions due to the top and bottom boundaries overlap and is significant for certain DG orientations. The second is a symmetry-dependent, in-plane unit-cell distortion that arises because the distorted morphology near the boundary has a different preferred unit-cell size and shape than the bulk. These results provide a thermodynamic portrait of the phase behavior of DG thin films.

Published under an exclusive license by AIP Publishing. https://doi.org/10.1063/5.0224767

I. INTRODUCTION

Materials discovery in soft matter has been advanced significantly through the study of block polymer self-assembly. Advancements in synthetic chemistry have enabled the creation of block polymers with an enormous variety of architectures and chemical compositions, and equally significant advancements in polymer field theory have predicted their equilibrium phase behavior with high accuracy. 1-4 The simplest system, a neat AB diblock polymer melt in the bulk, is now quite well understood, and much of contemporary block polymer research focuses on expanding the number of experimentally accessible phases using increasingly complex polymer systems, such as multiblock polymers in various architectures.³ Thin-film confinement is a particularly useful way to increase the system complexity, as many promising applications for block-polymer materials benefit from a thin-film geometry. Yet, only the simplest morphologies, cylinders and lamellae, are

well understood in thin films. It is thus of practical interest for a multitude of reasons to develop a broader understanding of the phenomena that affect the phase behavior of block-polymer thin films.

The promise of thin-film confinement as a design tool for materials discovery lies in its ability to generate stability windows for phases that are metastable in the bulk, for instance, perforated lamellae (PL), 10-12 as a consequence of fixed film thickness and/or preferential wetting at the top and bottom boundaries of the film.⁵ In these confined morphologies, the orientation of the phase relative to the substrate is an important property affecting the free energy. Lamella- and cylinder-forming phases in thin films have been studied extensively due to the potential utility of these phases for nanolithography. 7,8,13,14 Thin films of other phases—spherepacked phases and bicontinuous networks—are desirable for other applications, including nanoporous membranes, 15-19 electronic material templates, ^{18–21} and optical material templates, ^{22–}

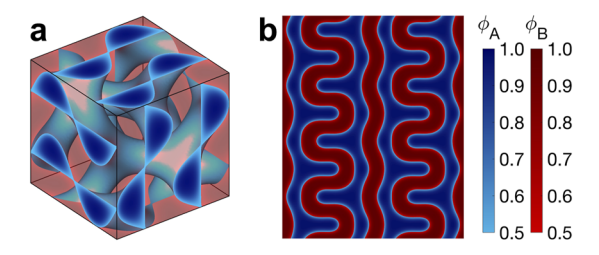


FIG. 1. The morphology of the DG phase in the bulk, computed using self-consistent field theory for an AB diblock polymer with A-block fraction $f_A=0.36$ and segregation strength $\chi N=20$. (a) The DG unit cell. The A domains are shown in blue, and the B domains are shown as semitransparent red. (b) The "double-wave" pattern that is often observed on the top surface of DG thin films, where the color represents the local composition as indicated by the colorbars. The pattern shown is that found on the bulk $(211)_{1/2}$ plane of DG, using the notation outlined in Sec. III.

though far fewer studies have characterized these phases under confinement.

The double-gyroid (DG) phase [Fig. 1(a)], a bicontinuous network phase that is stable in bulk AB diblock polymers over a narrow composition window, ^{29–32} is an important practical example of such a phase, and it is well-suited as a case study on confinement effects for geometrically complex phases. The morphology of DG in the bulk has been comprehensively characterized^{32–3} way down to the shape of the medial surface on which chain ends tend to be located³⁴ and the orientation of the chains relative to the A/B interface³⁶—providing a rich array of analytical tools that can also be used to describe the morphological effects of confinement. DG thin films have been observed experimentally in several studies, ^{27,28,37–42} meaning that theoretical predictions can be feasibly tested by experimentalists. Furthermore, in contrast to cylinders and lamellae, there is no intuitive reason to expect a DG thin film to form in a particular orientation because its three-dimensionally co-continuous morphology has no obvious location for a termination plane, such as a plane of mirror symmetry. A comprehensive description of DG thin films thus must consider all of the boundary effects that cause energetic differences between different termination planes.

In a prior work,⁴³ we determined the relative stability of DG thin films with various termination planes using self-consistent field theory (SCFT) calculations. This prior study focused on films confined between two nonpreferential boundaries containing an AB diblock polymer that forms DG in the bulk. At the film boundaries (which we refer to as "walls," although the calculations are also valid for unconfined films), we observed that the wetting angle—the angle between the A/B interface and the wall—is roughly 85° at all points on the wall, regardless of the termination plane. The DG morphology was thus distorted near the walls in order to achieve this preferred wetting angle regardless of the termination plane, a phenomenon which we referred to as "boundary frustration." Any distortions relative to the bulk morphology will be energetically unfavorable, so the termination plane in DG that requires the least distortion is expected to be the most stable. One particular termination plane with a "double-wave pattern" [Fig. 1(b)], which is oriented parallel to the (211) lattice plane, appears in nearly every DG thin film formed in experiments, ^{27,28,37-42} and our results indicated that this termination plane is indeed the most stable because it requires the least distortion to achieve the preferred wetting angle.

Our preliminary work⁴³ explained the relative stability of different DG termination planes but did not consider the stability of DG relative to other phases, nor did it consider the effect of preferential wetting on the phase behavior of the system. In the present contribution, we extend our previous analysis to address these questions of the broader phase behavior for thin films containing AB diblock polymers that form DG in the bulk. We begin by describing our methodology in Sec. II and our notation for labeling termination planes in DG in Sec. III. We then introduce a broad array of candidate phases in Sec. IV and describe how their free energies compare to DG, summarizing the overall phase behavior in a set of phase diagrams as a function of film thickness, block composition, and preferential wetting. A rigorous interpretation of these results requires an understanding of all significant contributions to the free energy in these thin films, so we summarize all known energetic effects in Sec. V, followed by a detailed description of one particular free-energy contribution that is especially relevant to DG thin films: constructive interference. Finally, in Sec. VI, we examine the morphologies of DG thin films in various orientations, describing the symmetry breaking that occurs due to thin film confinement and the resulting lattice distortions that can be expected relative to the bulk.

II. METHODS

A. Self-consistent field theory (SCFT)

The SCFT model used for all results herein has been described previously.⁴³ Therefore, we provide only a brief summary of the main equations and techniques. All results were generated using the C++ version of the open-source PSCF software.^{44–46}

We focus on a neat melt of monodisperse, conformationally symmetric AB diblock polymers confined to a thin film geometry. Let N be the total degree of polymerization of the polymer, and let b denote the statistical segment length for both species A and B. The calculation cell has volume V with periodic boundary conditions in each direction. At each position ${\bf r}$ in the unit cell, the average volume fractions of species A and B are denoted as $\phi_{\rm A}({\bf r})$ and $\phi_{\rm B}({\bf r})$, respectively. Within the unit cell, the polymers are confined to occupy only a predefined subvolume specified by a "mask" function $\phi_m({\bf r})^{47,48}$ such that

$$\phi_{A}(\mathbf{r}) + \phi_{B}(\mathbf{r}) = \phi_{m}(\mathbf{r}) \tag{1}$$

serves as the effective incompressibility constraint, while also enforcing thin-film confinement via the mask. We refer to the excluded regions of the unit cell, where $\phi_m(\mathbf{r})\approx 0$, as the "walls." In the film itself, $\phi_m(\mathbf{r})\approx 1$, indicating that position \mathbf{r} is occupied by polymers. For a thin film of thickness Δ with walls oriented normal to the z-direction, we choose $\phi_m(\mathbf{r})$ to be⁴⁸

$$\phi_m(z) = 0.5 \left(1 - \tanh \left(\frac{0.5(T-L) + |z - \frac{L}{2}|}{0.25t} \right) \right),$$
 (2)

where L is the unit cell size in the z-direction, $T = L - \Delta$ is the thickness of the excluded (wall) region of the unit cell, and t is the width of the narrow polymer/wall interface.

Within this unit cell, our SCFT calculations iteratively solve for a set of effective potential fields, $w_{\rm A}({\bf r})$ and $w_{\rm B}({\bf r})$, defined by the mean-field equations, ^{45,49}

$$w_{A}(\mathbf{r}) = \chi \phi_{B}(\mathbf{r}) + w_{A,\text{ext}}(\mathbf{r}) + \xi(\mathbf{r}),$$

$$w_{B}(\mathbf{r}) = \chi \phi_{A}(\mathbf{r}) + w_{B,\text{ext}}(\mathbf{r}) + \xi(\mathbf{r}),$$
(3)

where $\chi_{AB} \equiv \chi$ is an effective Flory–Huggins interaction parameter between species A and B, $w_{\alpha,ext}(\mathbf{r})$ is the external potential field felt by species α at position \mathbf{r} , and $\xi(\mathbf{r})$ is a Lagrange multiplier field that enforces Eq. (1). The external fields can be arbitrarily defined, and we use them here to introduce preferential wetting into the calculations. Specifically, we introduce Flory–Huggins-like interaction parameters χ_{wA} and χ_{wB} that represent the energetic effect of overlap between each species and the walls, and these parameters are used to define the external potential fields. 47,48

$$w_{A,\text{ext}}(\mathbf{r}) = \chi_{\text{wA}}[1 - \phi_m(\mathbf{r})],$$

$$w_{B,\text{ext}}(\mathbf{r}) = \chi_{\text{wB}}[1 - \phi_m(\mathbf{r})].$$
(4)

Because these external fields are defined to be proportional to $[1-\phi_m(\mathbf{r})]$, the external field is only felt by polymers within the polymer/wall interface, where they are either attracted toward or repelled from the wall depending on the values of $\chi_{\rm wA}$ and $\chi_{\rm wB}$.

The composition fields $\phi_A(\mathbf{r})$ and $\phi_B(\mathbf{r})$ depend on the effective potential fields $w_A(\mathbf{r})$ and $w_B(\mathbf{r})$, so in order to identify these potential fields, we must begin with an initial guess and iteratively update the fields until a set of fields is found that satisfies Eq. (3) self-consistently. 4,45,50 The field update algorithm that we use is Anderson mixing $^{51-53}$ with variable unit cell size, 54,55 where we have modified the unit-cell size optimization used for periodic crystals so that the film thickness is held constant, while unit-cell resizing can still occur in the plane of the film.

At each iteration, the composition fields must be calculated based on the current guess for $w_A(\mathbf{r})$ and $w_B(\mathbf{r})$. To determine the composition fields for a given set of potential fields, it is necessary to first solve for the "propagators" $q(\mathbf{r},s)$ and $q^{\dagger}(\mathbf{r},s)$ for the polymer chain in the effective potential fields. ^{4,45,50} The forward propagator $q(\mathbf{r},s)$ is a constrained partition function for the chain segment between contour positions 0 and s under the condition that contour position s is pinned at position \mathbf{r} . The backward propagator $q^{\dagger}(\mathbf{r},s)$ is the corresponding constrained partition function for the chain segment between contour positions s and N. To compute the propagators, we solve the modified diffusion equations for a continuous Gaussian chain model,

$$\frac{\partial q(\mathbf{r}, s)}{\partial s} = \left[\frac{b^2}{6} \nabla^2 - w_{\alpha(s)}(\mathbf{r}) \right] q(\mathbf{r}, s),
-\frac{\partial q^{\dagger}(\mathbf{r}, s)}{\partial s} = \left[\frac{b^2}{6} \nabla^2 - w_{\alpha(s)}(\mathbf{r}) \right] q^{\dagger}(\mathbf{r}, s),$$
(5)

where *s* denotes the position along the polymer contour (from 0 to *N*) and $\alpha(s)$ represents the species, A or B, at contour position *s*. These equations are solved starting from an initial condition of $q(\mathbf{r},0)=q^{\dagger}(\mathbf{r},N)=1$ using a pseudospectral method. 4,45,50,56,57

With these propagators, we can calculate the composition fields,

$$\phi_{A}(\mathbf{r}) = \frac{1}{NQ} \int_{0}^{fN} ds \ q(\mathbf{r}, s) q^{\dagger}(\mathbf{r}, s),$$

$$\phi_{B}(\mathbf{r}) = \frac{1}{NQ} \int_{fN}^{N} ds \ q(\mathbf{r}, s) q^{\dagger}(\mathbf{r}, s),$$
(6)

where *Q* is the total partition function,

$$Q = \frac{1}{\overline{\phi_{m}V}} \int d\mathbf{r} \ q(\mathbf{r}, N). \tag{7}$$

In the above expression for Q, $\overline{\phi}_m$ is the average value of $\phi_m(\mathbf{r})$ over the entire unit cell, representing the volume fraction of the unit cell that is occupied by polymers.

Equations (1)–(7) fully define a single SCFT solution. Starting from different initial guesses, different solutions can be obtained for the same polymer system. The relative stability of these solutions can be compared to predict the phase behavior of the system, which requires a calculation of the Helmholtz free energy using 4,45,50

$$\frac{F}{nk_{\rm B}T} = -\ln\left(Qe\right) + \frac{N}{\overline{\phi}_{m}V} \left\{ \chi \int d\mathbf{r} \, \phi_{\rm A}(\mathbf{r}) \phi_{\rm B}(\mathbf{r}) - \int d\mathbf{r} \left[w_{\rm A}(\mathbf{r}) - w_{\rm A,ext}(\mathbf{r}) \right] \phi_{\rm A}(\mathbf{r}) - \int d\mathbf{r} \left[w_{\rm B}(\mathbf{r}) - w_{\rm B,ext}(\mathbf{r}) \right] \phi_{\rm B}(\mathbf{r}) \right\}, \tag{8}$$

where *n* is the number of chains in the unit cell.

B. Calculation parameters

All SCFT calculations in this study were performed using an intermediate value of the segregation strength, $\chi N=20$. For simplicity, the top and bottom walls of each film have identical wetting parameters. The polymer/wall interaction parameter $\chi_{\rm wB}$ was set to zero, and preferential wetting was introduced by varying the parameter $\chi_{\rm wA}$ as needed. In our model, only the difference $\chi_{\rm wA}-\chi_{\rm wB}$ determines the resulting phase behavior because we enforce incompressibility and use the continuous Gaussian chain model, which is completely flexible. Any model with finite compressibility, which considers segment orientation, produces results that would depend on the absolute values of $\chi_{\rm wA}$ and $\chi_{\rm wB}$, not just the difference between them.

The mask function ϕ_m was defined for all calculations using a polymer/wall interface thickness $t=0.2N^{1/2}b$ and an excluded (wall) thickness $T\geq 0.4N^{1/2}b$, regardless of film thickness or phase, which are the same parameters used in several previous studies. ^{43,48}

To accurately resolve the polymer/wall interface, it was necessary to use a high-resolution grid in the direction normal to the film such that the spacing between gridpoints was at least five times smaller than the polymer/wall interface thickness t. The spacing between gridpoints along the axes parallel to the film did not need to be as small, and the values we used were about twice as large as in the normal direction. To solve the modified diffusion equations of Eq. (5), we discretized the chain into 200 contour points. In the Anderson mixing algorithm, we used 75 histories for most calculations. Some calculations, particularly in the (111) orientation,

converged better with a smaller number of histories (25 or 50). The error threshold used to establish convergence was a value of 1×10^{-6} for the relative norm of the residual vector, as defined in the PSCF documentation. ⁴⁴ The entire set of PSCF input files used for this study is available for download through the Data Repository for the University of Minnesota, containing the specific parameters used for every calculation.

C. Common-tangent calculations

It was necessary to compute many common tangent lines to predict terrace formation in thin films using our SCFT results. In some cases, the SCFT free-energy profiles exhibited a small degree of noise, which can lead to inaccurate results for a common tangent line. Therefore, before computing the common tangent line, we performed a spline fit on the data, using a small but nonzero amount of smoothing to eliminate the effect of the noise. This was done using SciPy's UnivariateSpline tool, where the smoothing parameter s was set to 1×10^{-7} . An example of a smoothed free-energy profile, along with the raw data used to generate the spline fit, is given in Fig. S2. All free-energy data shown herein have been smoothed using this technique.

After collecting all of our data, we identified that these somewhat noisy free-energy data were due to the extrapolation that we used to generate initial guesses for the next state point along a parameter sweep. Explicitly, the PSCF code uses a Lagrange polynomial to extrapolate the fields $w_{\rm A}({\bf r})$ and $w_{\rm B}({\bf r})$ at the next state point from the previous three solutions along the parameter sweep. This method proved to be somewhat unstable when varying film thickness in the parameter sweep, resulting in the noise. However, the noise generated by this extrapolation is at least an order of magnitude smaller than the relative free-energy differences that we observed between different film morphologies, so we do not believe that the noise caused any noticeable error in the phase diagrams generated from the data. Owing to the large computational cost for generating the original dataset, we chose not to repeat all of the calculations without the Lagrange polynomial extrapolation. Nevertheless, to confirm the validity of our existing dataset, we confirmed in Fig. S2 that the spline fitting that we used to draw common tangent lines was sufficiently similar to the result obtained when we recalculated the solutions without extrapolation (i.e., from a zero-order continuation method to generate the initial guess) for a representative state point.

D. 3D visualizations

We show many 3D composition profiles for block polymer thin films (e.g., Fig. 1), all of which were generated using the Polymer Visual tool. This tool reads the data output by PSCF and generates a variety of useful visualizations, which we have made publicly available. This tool uses the isosurface and isocaps functions in MATLAB to identify the isosurface on which $\phi_A(\mathbf{r}) = \phi_B(\mathbf{r})$ for a given SCFT solution and construct a 3D graphic of the result.

III. NOTATION USED TO DESCRIBE TERMINATION PLANES

We adopt a similar notation to our previous work⁴³ to label arbitrary planes through the bulk DG unit cell, in which we explicitly

denote both the orientation and the relative position of the plane along its normal direction. First, let d_{hkl} be the d-spacing between neighboring (hkl) lattice planes. A plane parallel to the lattice plane (hkl) is denoted as $(hkl)_{\tau}$, where τ is a fractional displacement away from the crystallographic origin such that τd_{hkl} is the distance from the origin to the plane $(hkl)_{\tau}$ along the direction normal to the plane. The planes at τ and $\tau+1$ are symmetry-equivalent by a Bravais lattice translation, so we only use $\tau \in (0,1]$. The crystallographic origin is defined by the space group. For all of the DG thin films described in this work, we use this notation to indicate the plane in the bulk that most closely corresponds to the termination plane in the resulting thin film. However, it is important to note that the thin-film morphology at the film boundary is distorted relative to the bulk, and the resulting domain pattern at the film boundary is sometimes quite different from the corresponding bulk pattern.

In general, a given plane through a bulk phase actually corresponds to two termination planes since either side of the plane can become the boundary of the film. When we refer to a termination plane $(hkl)_{\tau}$, we use the convention that the polymer-containing side of the boundary is on the side of the plane that contains the crystallographic origin. This creates ambiguity when the plane contains the origin (when $\tau = 0$), which is why we use $\tau \in (0,1]$ to refer to a particular termination plane rather than $\tau \in [0,1)$. (Note that this differs from our previous work,⁴³ where we used $\tau = 0$.) Also by convention, we choose to refer only to the termination plane at the top boundary of the film. The symmetry-equivalent termination plane at the bottom boundary is $(hkl)_{-\tau}$ as long as the bulk space group has an inversion center at the origin, which is the case for all phases studied herein. It is left implicit for the remainder of this text that the plane $(hkl)_{-\tau}$ is used at the bottom boundary in any film that we describe as having $(hkl)_{\tau}$ termination planes.

Finally, we note that any given termination plane will have infinitely many other planes that are morphologically equivalent to it by symmetry, related by lattice translations and space-group symmetry. The spacing between these symmetry-equivalent planes is unique to each orientation (hkl). We treat two planes as symmetryequivalent termination planes as long as the shapes of the polymer domains are identical on the side of the plane that contains the origin, even if they are shifted, rotated, or mirrored in-plane relative to one another. For example, the set of planes $(111)_{n/4}$, where n is any positive integer, are symmetry-equivalent in the $Ia\overline{3}d$ space group of the DG phase.⁴³ Rather than using a generalized notation— $(111)_{n/4}$ in this case—to refer to a set of symmetry-equivalent planes, we will use the plane with the smallest positive value of τ as the "characteristic plane" representing the whole set, which is $(111)_{1/4}$ in this example. Table S1 lists all characteristic planes used in this study along with the full sets of symmetry-equivalent termination planes that they represent.

IV. PHASE BEHAVIOR

A. Candidate phases

To describe the phase behavior of a block polymer system using SCFT, we must compare the free energies of all candidate phases that are likely to have a window of stability. In thin films, each unique morphology of a given phase (defined by its termination planes)

must be treated as if it is an independent phase since the location of the film boundary has a significant effect on the resulting free energy. The complete set of candidate morphologies considered in this study is shown in Fig. 2. For reasons explained further below, we use identical termination planes on both the top and bottom boundaries in all films so that each SCFT calculation corresponds to only one termination plane.

The set of morphologies in Fig. 2 were chosen because they are the most likely to be stable in thin films near the DG stability window. We consider lamellae (L) and hexagonally packed cylinders (C) as candidate phases because they are the phases immediately adjacent to DG on the bulk phase diagram. 30 We also include perforated lamellae (PL), a network-like structure that is known to be closely metastable to DG in the bulk30 and has been observed in thin films of block polymers that form bulk network phases. 61,62 For simplicity, we consider only the abab-type stacking of PL, as the abcabc stacking is so energetically similar that it can be considered degenerate for our purposes.³⁰ For each of these candidate phases, the termination planes were chosen to include any plane of mirror symmetry, along with any plane that maximizes or minimizes the area fraction of either species (since these planes will be favored in films with preferential wetting at the film boundaries). One exception is that we did not consider PL oriented perpendicular to the film because this orientation has not been observed experimentally and is not expected to be stable. We did, however, include a mixed phase, denoted as PLL, which is a perforated lamellar phase with a nonperforated lamella of species A at each wall, which we find to be more stable than PL when the film boundaries are highly Apreferential. For clarity, the three different termination planes for parallel-oriented cylinders in Fig. 2 are drawn onto the bulk unit cell in Fig. S3.

To choose appropriate termination planes for DG, we followed the same approach described in our previous work, ⁴³ but extended to films with preferential wetting. We considered only the four orientations observed experimentally: ^{38,63} films with the (211), (001), (111), and (110) lattice planes oriented parallel to the substrate. We tested eight unique, evenly spaced termination planes in each orientation, using the bulk DG morphology to construct the initial guess for each SCFT calculation. From the converged solutions, we identified those that are most stable at their optimal film thickness and included them in the list of candidate morphologies shown in Fig. 2. We performed this procedure for nonpreferential walls previously, ⁴³ and the procedure was repeated here for walls that are highly A-preferential and walls that are highly B-preferential, at $\chi_{\rm wA} = -10$ and 10, respectively, to identify the set of candidate phases to be used at intermediate values of $\chi_{\rm wA}$. ($\chi_{\rm wB}$ was held at 0 for all calculations.)

As shown in Fig. 2, the DG termination planes in our set of candidate morphologies include $(211)_{1/2}$, $(001)_{1/8}$, $(111)_{1/4}$, and $(110)_{1/4}$, which were shown in our earlier work to be the most stable termination planes in their respective orientations when located against nonpreferential boundaries.⁴³ $(211)_{1/2}$, the termi-

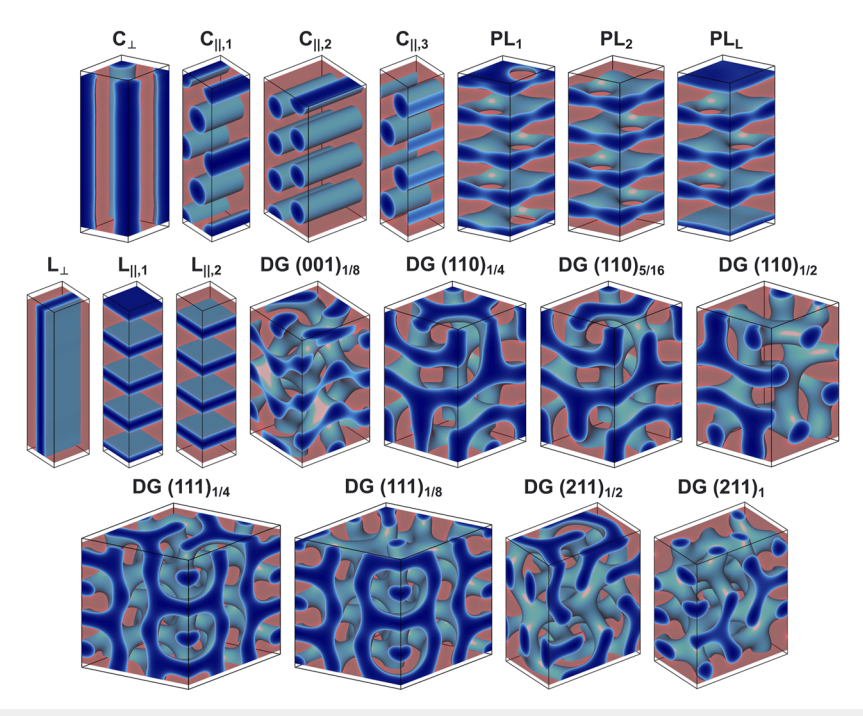


FIG. 2. The full set of candidate morphologies. All images are converged SCFT solutions at A-block fraction $f_A = 0.36$ and segregation strength $\chi N = 20$ in films between nonpreferential boundaries. For each morphology, a single crystallographic unit cell is shown. In each image, dark blue represents the domain rich in species A, and the semitransparent red region is the domain rich in species B. The light blue surface in the unit cell interior is the A/B interface. The empty space at the top and bottom of the unit cell is the region occupied by the confining walls of the film in the SCFT calculation.

nation plane with the double-wave pattern [Fig. 1(b)] that is very common in experiments, ^{27,28,37–42} was the most stable from among these four against a nonpreferential boundary. We find that these termination planes are the most stable in their respective orientations when placed between highly A-preferential walls as well. We also include $(110)_{5/16}$, a termination plane that is structurally similar to and nearly degenerate to (110)_{1/4}, as demonstrated in Fig. S4. Three additional DG termination planes are included as well, all of which were found to be the most stable in their respective orientations when placed between strongly B-preferential walls. These are the $(211)_1$, $(111)_{1/8}$, and $(110)_{1/2}$ termination planes. Note that the morphology of $(110)_{1/2}$ -terminated films is particularly distorted relative to the bulk, with non-bulk-like elongated struts near the film walls that intersect with the wall like a perpendicularly oriented cylinder. Despite these distortions, we found that this was the most stable morphology for a (110)oriented film between B-preferential boundaries, so we included

It is possible that other unknown morphologies may be energetically competitive with those shown in Fig. 2 for the polymer systems studied here. Various techniques have been developed to identify such unknown phases, 64-67 but they are computationally expensive and are not guaranteed to identify novel morphologies with windows of stability. The purpose of this study is to improve the understanding of known diblock polymer phases in thin films, so we do not endeavor to identify novel morphologies that may be competitive, though this is a promising avenue of research for future studies.

B. Identifying the stable phase

Before comparing the free energies of these various films, we must make an important distinction between confined and unconfined films. A confined film is one in which both boundaries are rigid, for instance, when a polymer melt is confined in a slit. By contrast, an unconfined film sits on a rigid substrate but has one interface that is not rigid, typically because it is open to air. In unconfined films, terrace formation can occur, where the film splits into thicker and thinner regions rather than maintaining a uniform thickness. ^{47,68-70} This occurs when the average film thickness is incommensurate with the periodicity of the preferred phase in the direction normal to the film. It is energetically preferable to form terraces that each has commensurate film thicknesses, rather than stretching or compressing the morphology to accommodate the incommensurability.

In this study, we focus on unconfined films, which are more common experimentally. Our SCFT calculations, however, model confined films. Fortunately, Matsen⁴⁷ demonstrated that a commontangent construction can be used to calculate the free energy of an unconfined film with terraces based on the free energy of confined films. As a resource to the reader, the supplementary material contains a pedagogical explanation for implementing the commontangent construction for terraced thin films using data from SCFT, along with a detailed thermodynamic derivation of the commontangent construction. For conciseness, only the essential details are described here.

The common-tangent construction is performed on a plot of the excess free energy per unit area of the film as a function of film thickness. As an example, Fig. 3(a) shows this property for a confined film (black), where the film thickness is fixed at some value of Δ , and an unconfined film (blue), where the film forms terraces if the average film thickness Δ is not commensurate. In both cases, the films have $(211)_{1/2}$ termination planes and the polymer forms DG in the bulk ($f_A = 0.36$ and $\chi N = 20$). The confined-film free energy has local minima when the film thickness is commensurate with d_{211} , the bulk spacing between $(211)_{1/2}$ termination planes, and exhibits local maxima halfway between commensurate thicknesses. As film thickness increases, the film morphology undergoes a step change in the termination plane at each of these local maxima to the next adjacent $(211)_{1/2}$ plane, minimizing the degree of incommensurability. The free energy of the unconfined film is determined by drawing common tangent lines between adjacent local minima on the free energy of the confined film. Blue dots indicate the points of tangency, which are the film thicknesses of the terraces that will form when the average film thickness is incommensurate with d_{211} . For a terraced film, the area fraction of each terrace height can be obtained using a lever

One important detail in Fig. 3(a) is that a lower value of excess free energy per unit area is observed at very small film thicknesses—a feature that arises due to overlapping distortions near the top and bottom boundaries, which we will describe in more detail in Sec. V. Because the leftmost local minimum is lower than the rest, a common tangent line could be drawn with lower free energy than the lines shown in the figure if the tangent line is drawn between the leftmost local minimum and the rightmost local minimum. However, we do not use such a common tangent line because it would represent terrace formation with very thin terraces and very thick terraces. To our knowledge, this has not been observed experimentally, likely due to kinetic limitations. Therefore, we draw common tangent lines only between adjacent local minima on the free-energy diagram.

Continuing with this example, Fig. 3(b) shows how the unconfined free energy in Fig. 3(a) compares to that of other phases in various orientations. We omit other DG orientations because our previous work⁴³ has shown that (211)_{1/2} is the most stable DG termination plane for this thin-film system, and we show only the films with the lowest free energies from among the other morphologies shown in Fig. 2. At low film thicknesses, we see that $C_{\parallel,1}$ is the most stable morphology, though it is nearly degenerate with PL1. As thickness increases, DG quickly becomes more stable than any competing phases. This is expected since DG is the phase that is most stable in the bulk, and increasing the film thickness increases the fraction of the film that is "bulk-like" in the middle of the film. In addition, near the transition from cylinders to DG, a common tangent line can be drawn between $C_{\parallel,1}$ and DG (211)_{1/2} that is more stable than any other line on this diagram, though it is not shown in Fig. 3(b). Along this line, the most stable film will be a terraced film with $C_{\parallel,1}$ in the thinner terraces and DG (211)_{1/2} in the thicker

To show how large the free-energy differences are between these various morphologies, it is also useful to look at the excess free energies per polymer, rather than per unit area, as the free energy per polymer is the property most commonly reported in bulk SCFT studies. This property is highly dependent on film thickness [see Fig. S1(a)], so we can only compare values across morphologies at the same film thickness. Figure 3(c) shows one such set of free energies

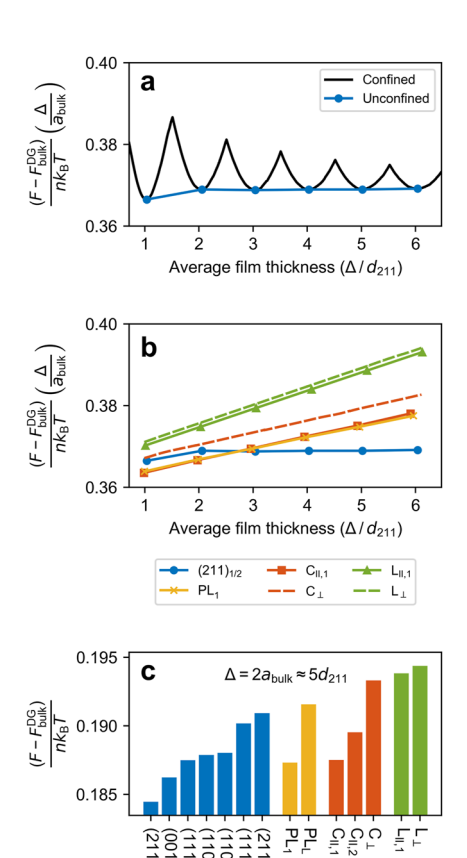


FIG. 3. An example of thin-film free-energy analysis, for a film between nonpreferential walls containing a diblock polymer with $f_{\rm A}=0.36$ and $\chi N=20$. (a) The excess free energy per unit area of the film, relative to the bulk DG free energy $F_{\rm bulk}^{\rm DG}$, for a confined (black) and unconfined (blue) DG thin film with (211) $_{1/2}$ termination planes. Dots indicate the film thicknesses of the resulting terraces. (b) The excess free energy per unit area for various unconfined films. For terrace-forming films, markers denote the thicknesses of the resulting terraces. (c) The excess free energy per polymer for unconfined films with average film thickness $\Delta=2a_{\rm bulk}$, for all morphologies in our study that were within $10^{-3}k_{\rm B}T$ per chain of the most stable morphology.

for unconfined films at an average film thickness $\Delta = 2a_{\rm bulk} \approx 5d_{211}$, a state point at which DG films with (211)_{1/2} termination planes are the most stable, as evident in Fig. 3(b). In this bar chart, we show the free energies for all morphologies tested that have free energies per polymer within $10^{-3}k_{\rm B}T$ of the most stable film. Most of the morphologies that we tested meet this criterion; only those with the majority block covering the entire wall ($C_{\parallel,3}$, PL_2 , and $L_{\parallel,2}$) are omitted from the figure. The minority block is entropically preferred at the boundaries, 10,11,71-74 which explains the metastability of these morphologies. The figure reveals that there are many morphologies that are closely metastable, but that (211)_{1/2}-terminated DG is clearly the most stable.

Let us now return briefly to the morphologies in Fig. 2. As mentioned above, the set of morphologies studied here only contains films with identical termination planes on the top and bottom

boundaries. This is a simplification that is permitted only when two particular conditions are met. The first is that the film boundaries must have identical properties; the wetting behavior ($\chi_{\rm wA}$ and $\chi_{\rm wB}$) and polymer/wall interface width (t) are the same at the top and bottom boundaries in all of our SCFT calculations. The second condition is that we focus only on unconfined films that can form terraces. If both of these conditions are met, then the most stable film will always have the same termination plane on the top and bottom boundaries within a single terrace, though the morphology in the thicker terrace may still be different from that in the thinner terrace. We restrict this study to such systems for exactly this reason; not only does it reduce the parameter space significantly if all films have identical termination planes on both boundaries, but—more importantly—it leads to a dataset where each SCFT calculation provides information about a single termination plane, rather than the mixed effects of two dissimilar termination planes. These results thus allow us to understand the morphology that is energetically preferred at a single boundary and identify the reasons for its stability, which will ultimately prove valuable for understanding the behavior of films with asymmetric boundaries as well.

C. Phase behavior: Nonpreferential boundaries

Having described the methodology for determining the phase behavior, we now present a set of phase diagrams that demonstrate how the equilibrium film morphology changes as a function of two key properties: block fraction and preferential wetting. We begin by considering unconfined films between two nonpreferential boundaries, focusing on the effect of minority-block volume fraction f_A and (average) film thickness Δ in the vicinity of the bulk DG stability window, which extends from $f_A = 0.338$ to 0.375. The phase diagram for these films is shown in Fig. 4. For all morphologies on the diagram other than L_{\perp} , terraces are expected to form when the film thickness is incommensurate with the preferred spacing between termination planes. The commensurate thicknesses, which are also the thicknesses of the terraces that will form from films of incommensurate thickness, are indicated on the diagram by dashed lines. A vertical tie line can be drawn between neighboring dashed lines and/or thin black lines to determine terrace heights for a film with a given average thickness, and a lever rule along these tie lines can be used to compute the area fraction of the film covered by each terrace height. Similarly, the white regions of the phase diagram represent films in which terraces are expected to form between unlike morphologies; the morphologies and heights of each terrace formed inside these two-phase regions can also be predicted using vertical tie lines. Finally, a thick black line marks the phase boundary with L₁ to indicate that it does not form terraces with neighboring morphologies. This is because the L_⊥ morphology does not have commensurate/incommensurate thicknesses, as all polymer chains are oriented parallel to the boundaries. The excess free energy per unit area of this morphology has no local minima [see Fig. 3(b)], and no common tangent lines

The phase diagram reveals that DG with $(211)_{1/2}$ termination planes is stable at film thicknesses as small as about $1.2a_{\rm bulk}^{\rm DG}$, which is the DG morphology that has been most often observed in experiments, $^{27,28,37-42}$ but is notably thinner than the thinnest

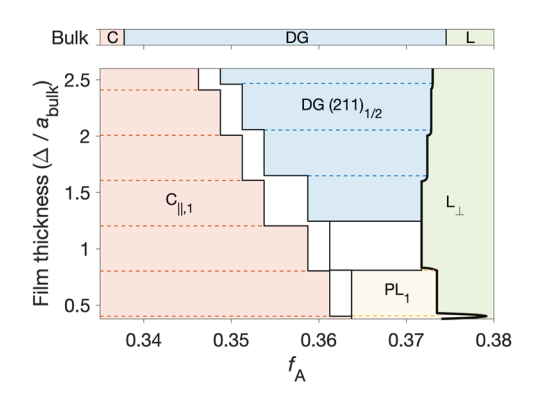


FIG. 4. Phase diagram for unconfined block polymer thin films with $\chi N=20$ in the absence of preferential wetting at either boundary, as a function of average film thickness Δ and minority-block fraction f_{Δ} . The bulk phase behavior is shown at the top of the figure. The labels on the diagram correspond to the morphologies shown in Fig. 2. The data points used to construct the diagram are shown in Fig. S5. A thick black line on the L_{\perp} boundary is used to indicate that terraces do not form for this phase.

DG thin films fabricated to date. When the film thickness goes below the DG stability window, the film will instead form $C_{\parallel,1}$ or PL₁, depending on f_A . PL is not stable in the bulk, but is stabilized by geometric confinement in very thin films. Aside from the gradual narrowing of the DG stability window as film thickness decreases and the small stability window of PL, the phase behavior is not significantly altered relative to the bulk. This is not surprising, given the only difference that we have introduced between the bulk and these films is the presence of two flat, noninteracting boundaries. In addition, note that there is a small region in the lower-right corner where the PL₁ stability window juts out into the L_{\perp} stability window, which appears at a commensurate film thickness where PL₁ is particularly stable, as illustrated in more detail in Fig. S7.

D. Phase behavior: Preferential boundaries

Perhaps more interesting is the effect of preferential wetting on the phase behavior of thin films, which is known to be substantial⁷⁵ but is quite poorly understood for DG films. The wetting conditions at the film boundaries depend on the relative interfacial tensions between each monomer species and the chemical species on the other side of the boundary, which may be a substrate, a solvent vapor, air, or another fluid. These interfacial tensions can be tuned by, for example, depositing a surface modification layer on the substrate before film deposition or applying a top coat at the polymer/air boundary. 41,78 Figure 5 shows the phase diagram for diblock polymers at $f_A = 0.36$, in the middle of the bulk DG stability window, as a function of preferential wetting and film thickness. In these films, we held $\chi_{\rm wB}$ = 0 and varied $\chi_{\rm wA}$ from -10 to 10. Although it is difficult to quantitatively relate the value of $\chi_{\rm wA}$ to an experimentally measurable property, the phase diagram provides a qualitative portrait of the expected phase behavior. Furthermore, we can see from the phase diagram that morphologies with a complete (or nearly complete) wetting layer at the walls are

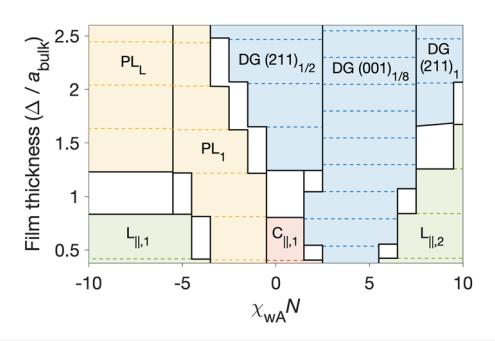


FIG. 5. Phase diagram for unconfined block polymer thin films with $f_A=0.36$ and $\chi N=20$ as a function of average film thickness Δ and preferential wetting at the film boundaries $\chi_{wA}N$, where $\chi_{wB}=0$. The labels on the diagram correspond to the morphologies shown in Fig. 2. The data points used to construct the diagram are shown in Fig. S6. One phase boundary on the right-hand side of the diagram has a slight positive slope, which is explained in Fig. S8.

stabilized at $\chi_{\rm wA}=\pm 10$, which provides a reasonable sense of the strength of the preferential interactions considered here. As in Fig. 4, the thicknesses of stable terraces are indicated using dashed lines, and terrace formation can be predicted using vertical tie lines; the white regions of the diagram indicate terrace formation between nonsimilar morphologies.

Figure 5 reveals a stability window for two termination planes in DG that have not been observed experimentally in diblock polymer thin films. Specifically, the $(001)_{1/8}$ termination plane is stable against a modestly B-preferential interface, and the (211)₁ termination plane is stable against a strongly B-preferential interface. Similar to $(211)_{1/2}$, these two termination planes can accommodate the film boundary with relatively little distortion of the bulk DG morphology (i.e., relatively low boundary frustration), but these termination planes have a smaller A-block area fraction at the film boundaries, especially on the (211)₁ plane. Their low A-block area fraction explains their metastability against a nonpreferential boundary since the minority block is modestly favored against such a boundary due to chain-end entropy (see Sec. V), and it also explains their stability against B-preferential boundaries since the wetting preference for B at the boundary quickly becomes a larger contributor to the free energy than the entropic preference for A. It is curious that these two termination planes have not been observed in any experiments, while others including $(111)_{1/4}$ and $(110)_{1/4}$ have been observed^{37–39,63} even though we do not predict a window of stability for them. This may be due to factors such as conformational asymmetry or polymer dispersity that are not considered in our model, or the films observed experimentally may be kinetically trapped in a metastable state. The latter is especially likely, given that most of these films are fabricated using solvent vapor annealing, which often traps nonequilibrium structures.7

We also see in Fig. 5 that DG is quickly destabilized by A-preferential interfaces, with PL favored to form instead. PL_1 is already closely metastable for nonpreferential interfaces, and it achieves much greater surface coverage of species A at the interfaces than DG. Thus, a small energetic preference for species A at the interfaces is enough to stabilize PL_1 . It also requires relatively minimal distortion for PL_1 to transition to PL_L to accommodate

strongly A-preferential interfaces, making PL_L the morphology that is expected to form in such cases.

This transition from PL₁ to PL_L demonstrates that the formation of a complete wetting layer is a necessary condition for stability of a morphology against a strongly preferential interface, and the energetically preferred morphology will be that which can achieve a complete wetting layer with the least distortion. (211)₁-terminated DG films are an exception based on Fig. 5, as they have a small amount of A monomer at the interface, but the stability window of these DG films will only continue to get overtaken by $L_{\parallel 2}$ (which achieves a complete wetting layer) as $\chi_{\rm wA}N$ exceeds 10. This raises an interesting question, which we do not attempt to answer here: Are there certain planes in DG that might be able to smoothly transition to a complete wetting layer without incurring a significant energetic penalty? Ultimately, SCFT may not be the most effective tool for predicting the morphology of a diblock polymer thin film near a strongly preferential interface since these interfaces are likely stabilized in many cases by defects, amorphous regions, or morphological discontinuities (grain boundaries) that are not easy to model.

E. Limitations of the model

Real block polymers will inevitably exhibit phase behavior that differs from that described here since the polymer system in our model is idealized. Conformational asymmetry and dispersity are present in every block polymer system—though often only to a small extent—and neither effect is included in this study. Indeed, a highly disperse A block has been shown to result in DG formation at $f_A = 0.51$ in thin films, much higher than any f_A values considered here.⁴² Additionally, the continuous Gaussian chain model represents a completely flexible polymer, leading to the physically inaccurate condition where the persistence length of the polymer is smaller than the width of the polymer/wall interface;⁵⁹ a polymer with finite persistence length located next to a rigid wall will exhibit nematic ordering of chain segments against the wall, which is absent in our calculations. Finally, our incompressible model does not consider the possibility of dewetting, which may occur in some films with very small film thicknesses. The phase behavior we describe here thus represents a starting point from which to understand DG thin films, and the effects described in this paragraph will need to be more closely studied in order to construct a rigorous prediction of the phase behavior for any given experimental system. It will also be necessary to investigate the effect of changing χN , which was not a variable in this

SCFT provides access to the morphology and energetics of polymer systems at equilibrium, but provides no information about the kinetics or path-dependent phase formation that is often observed experimentally. Although this may at first seem to be a limitation, this information about the true equilibrium state of a system is invaluable for interpreting experimental results; if a film forms a phase that is not predicted to be globally stable, then it was probably trapped in a metastable state by a processing step and may even undergo a slow phase transformation to the globally stable phase over the course of weeks or months. For instance, it is unclear why DG thin films fabricated using solvent vapor annealing exhibit various orientations with uniform film thickness, ^{37,39,63}

while similar films annealed in the absence of solvent vapor form terraces and favor only the (211) orientation. ⁴² With knowledge of the equilibrium phase for these films, we can begin to disentangle the path-dependent effects of solvent vapor annealing and other processing steps from the thermodynamic incentive to minimize the overall free energy.

V. CONSTRUCTIVE INTERFERENCE BETWEEN BOUNDARY DISTORTIONS

One reason why the DG phase is such a useful case study for understanding the effects of thin-film confinement is that it is morphologically complex; the three-dimensionally bicontinuous domains and the A/B interfaces with saddle curvature make it difficult to intuit the consequences of confining DG between flat boundaries. Yet, DG is also highly symmetric, greatly reducing the number of potential film morphologies and making it a tractable system to characterize. The morphological complexity implies that most—if not all-significant confinement effects that appear in block polymer thin films will appear in DG thin films in at least one orientation. Indeed, we find that all known confinement effects are observed in DG thin films, and certain effects that are nonexistent or negligible in thin films of lamellae or hexagonally packed cylinders are highly consequential in DG thin films. One effect in particular, which we refer to as constructive interference, contributes significantly to the free energy of DG films, especially at low film thickness, but is largely irrelevant for other phases. In this section, we first provide a brief overview of the known confinement effects that are of consequence to the free energy of the films in this study, followed by a more in-depth discussion of constructive interference by way of an example.

Consider, as we did in Fig. 3, the excess free energy per unit area of an arbitrary thin film, where "excess" is defined relative to the DG phase in the bulk. For a film in a phase other than DG, the first and most important contribution to the excess free energy per unit area is the relative difference in bulk free energy, which scales linearly with film thickness because the bulk free energy per unit volume is a constant and the volume of the film per unit area scales linearly with film thickness. In Fig. 3(b), the free energy of all phases other than DG increases as a function of thickness because of this contribution.

Another set of free-energy contributions can be described as "single-boundary effects." These represent the contributions from each boundary that would arise in the limit of large film thickness—when the interior of the film is entirely bulk-like—so they are independent of one another, are not a function of film thickness, and vary with each unique termination plane. There are five known single-boundary effects in the literature. The first effect is the wetting energy of each monomer species at the boundary, which depends on the interfacial tensions between each species and the boundary as well as the area fractions of each monomer species at the boundary.⁵ gives rise to preferential wetting. Second, chain ends are entropically favored near the boundary, 10,11,71-74 which leads to a preference for the minority block at the boundary since minorityblock domains have a higher chain-end density. Third, there is a negative line tension that forms where the A/B interface intersects the boundary due to the reduction of A/B interactions

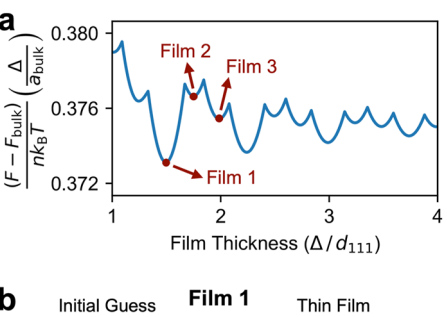
near the boundary, which favors the maximum amount of contact between the A/B interface and the boundary. ^{47,74,83} Fourth, monomer species with shorter statistical segment lengths are entropically favored at the boundary in polymer systems with conformational asymmetry. ^{59,86,87} Fifth, the presence of the boundary can induce distortions relative to the bulk that increase the free energy. ⁴³ The extent of these distortions depends on the termination plane and on preferential wetting, referred to as "boundary frustration," which was shown to be significant for DG thin films in particular.

The final important contribution to the excess free energy per unit area is the "interference" that arises when the distortions at the top and bottom boundaries overlap. 47,88 This occurs primarily when the film thickness is very low and/or when the distortions needed to accommodate the boundary are significant, which is the case for some metastable orientations of DG. 43 Depending on the morphology and the film thickness, the distortions can mutually stabilize or destabilize one another, which we refer to as constructive or destructive interference, respectively (a naming convention first used by Pickett and Balazs 88). This interference has been observed previously in SCFT calculations for very thin films of perpendicular lamellae between preferential boundaries, 47,88 but is much more significant and appears at much higher film thicknesses in the DG thin films in this study.

Figure 6 provides an illustrative example: DG thin films with (111)_{1/4} termination planes and nonpreferential boundaries. These films are metastable relative to those with (211)_{1/2} termination planes, largely because they require greater distortions to accommodate the boundaries. Figure 6(a) shows the excess free energy per unit area for confined films with these termination planes as a function of film thickness. The figure shows a trend that at first seems quite unexpected: films with neighboring termination planes (e.g., the three points labeled "film 1," "film 2," and "film 3") have very different free-energy minima. The morphology of the films at each boundary is the same, so the free-energy contributions due to single-boundary effects are constant. Therefore, the difference in free energy between neighboring commensurate films indicates that these films exhibit either constructive or destructive interference, depending on the spacing of their termination planes.

Figures 6(b)-6(d) illustrate that this interference can be observed directly in the morphology of the thin films. Figure 6(b) shows a 3D view of the SCFT initial guess (which is simply the bulk morphology) alongside the converged solution for the point labeled "film 1" in Fig. 6(a), which has a very low free energy indicative of constructive interference. On the top and bottom of the film, there are two tripod-like structures where the minority (blue) domain intersects the film boundary. Neither of these tripod-like structures are bisected through the middle by the film boundary; instead, one of the structures is centered slightly below the boundary, while the other is centered slightly above the boundary and is therefore mostly cut off by the boundary. This is more clearly evident in the 2D contour slice shown below the 3D graphic, where we have chosen a slice that goes directly through the center of each of these tripods.

Against a nonpreferential boundary, a gyroid strut is most stable when it is bisected, essentially a half-cylinder located on the boundary, due to the preferred wetting angle of roughly 85°.



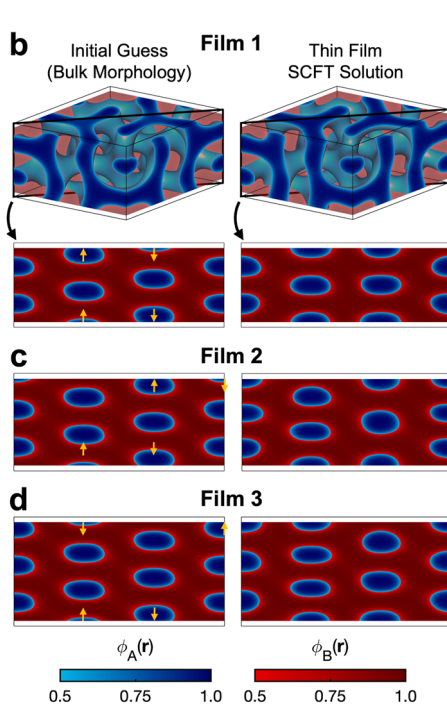


FIG. 6. Constructive and destructive interference of boundary distortions. (a) The excess free energy per unit area of confined DG thin films between nonpreferential boundaries with (111)_{1/4} termination planes as a function of film thickness. (b) The initial guess (the DG bulk morphology) and the resulting SCFT solution for the film labeled "film 1" in (a). A 3D view of one unit cell is shown, where blue is the species A domain and semitransparent red is the species B domain, with empty regions on the top and bottom representing the walls used to impose confinement. Below, the 3D views are 2D slices through the middle of the unit cell (the black squares on the 3D views), with colors corresponding to the colorbars (bottom). Arrows indicate the direction that the A domains shift to accommodate the boundary, showing that constructive interference occurs. (c) and (d) Corresponding 2D slices for the films labeled "film 2" and "film 3" in (a), respectively, both of which instead exhibit destructive interference.

Therefore, these tripod-like structures need to shift up or down relative to the bulk in order to be bisected by the boundary and achieve the most stable conformation. The direction of shift for each tripod is indicated by orange arrows in the figure. On the right side of Fig. 6(b), we show the thin-film SCFT solution, which shows that these upward/downward shifts do indeed occur. Importantly, tripod-like structures that are directly above/below one another shift in the same direction in this thin film. The distortions at the top and bottom boundaries of the film therefore complement

each other and constructive interference occurs, lowering the free energy.

By contrast, films 2 and 3 experience destructive interference, in which the distortions required at the top and bottom boundaries clash and cause further destabilization. This is visualized in Figs. 6(c) and 6(d), which show the same 2D slices as Fig. 6(b) but for these thicker films. The upward and downward shifts of the tripod-like structures now go in opposite directions for tripods that are aligned above/below one another. Two of the tripods in these films have no tripod above/below them, so they are shifting upward or downward, while the aligned morphology at the opposite boundary would rather not shift up or down at all. In these films, the free energy is increased due to this interference.

The effect of constructive interference is also evident in Fig. 3(a) for films with $(211)_{1/2}$ termination planes. The leftmost local minimum in the figure has a lower excess free energy per unit area than any other local minima because the two boundaries are close enough together that the distortions at the boundaries overlap. However, these termination planes do not induce significant distortion, 43 so the distortions induced by the boundaries do not overlap for thicker films like they do in the (111) orientation. Similar behavior is observed for (001)-oriented films, which exhibit constructive interference below thicknesses of $\approx a_{\text{bulk}}$. Curiously, (110)-oriented films do not exhibit noticeable interference effects in their free-energy profiles [Fig. S4(a)], even though they exhibit greater boundary frustration than the other orientations.⁴³ Qualitatively, these films appear to be highly distorted relative to the bulk in the region near the boundaries, but these distortions do not permeate deep into the film like they do in (111)-oriented films. This implies that a film with high boundary frustration will not necessarily exhibit interference depending on whether the distortions induced by a boundary are highly localized near the boundary.

VI. SYMMETRY BREAKING AND IN-PLANE DISTORTIONS

There is one other informative output of our SCFT calculations that has not yet been discussed: the optimized lattice parameters of the unit cell. We require in every calculation that the lattice basis vectors $\bf a$ and $\bf b$ are oriented parallel to the film and that the third lattice basis vector $\bf c$ is oriented perpendicular to the film. The length of the latter defines the film thickness, so it is not allowed to vary. The lengths $a = |\bf a|$ and $b = |\bf b|$ are independent of the confining geometry, as is the angle y between vectors $\bf a$ and $\bf b$. Thus, in each calculation, we allow a, b, and y to relax to the value that minimizes the free energy per polymer. In this section, we examine these lattice parameters for DG thin films, revealing a complex relationship between symmetry breaking, in-plane distortions, and the concept of constructive interference, all of which can be distilled down to a relatively simple explanation.

Before showing the results themselves, we begin by presenting the key idea revealed by the results: the region of the film near a film boundary often has a preferred unit cell shape that is different from the bulk due to the fact that the morphology of the phase itself is distorted in this region. This is intuitive, but it is nontrivial to isolate this effect from the many other boundary effects that all simultaneously occur within a thin film. More complicated still is the challenge of predicting which parameters will distort for a given film and how much they will distort. Much of this complication boils down to the fact that a single boundary cannot be isolated from the rest of the film; each film has two boundaries that, in general, will prefer different distortions to the unit cell, along with the bulk-like region in the middle of the film that would prefer no distortion relative to the bulk. In the limit of large film thickness, the unit cell size in the plane of the film will be the same as the corresponding periodicity in the bulk because the large bulk-like region in the middle of the film will dominate the overall free energy that is used to optimize the unit cell size. However, at lower film thicknesses, the bulk-like region is small, so the unit cell shape will change somewhat if it will further stabilize the boundary. Implicit in this description is the idea that in-plane distortion of the unit cell is a form of constructive interference between the top and bottom boundaries, and any stabilization achieved by in-plane distortions will serve to lower the free energy.

The directions of the distortions that we observe depend on the phase's orientation in the film. More specifically, the distortions can be predicted based on the film's crystallographic symmetry. The film boundary breaks the bulk symmetry of a phase, reducing a threedimensional set of symmetry operations that describes the bulk phase down to a two-dimensional set, with symmetry operations permitted only if they do not affect the location of the boundaries. Therefore, it is often convenient to describe the symmetry of a thin film using a 2D plane group, rather than a 3D space group. The plane group for a given film only depends on its orientation relative to the bulk, and it prescribes exactly which in-plane distortions are allowed for the film based on its symmetry. However, an exception arises when the top and bottom boundaries are identical, with the same wetting properties and the same termination plane, in which case there are permitted symmetry operations that relate the top boundary to the bottom boundary as well. A 3D space group is required to describe the symmetry of such a film, and the space group depends on which bulk plane corresponds to the midplane of the film (since the symmetry operation relating the two boundaries must lie on the film's midplane). In the supplementary material, we provide a procedure for determining the plane group or space group for a given film.

Let us consider the four orientations of DG considered in this study, focusing (for now) on films with nonsimilar boundaries that only have 2D plane-group symmetry. In each orientation, the plane group dictates which distortions are permitted. (001)-oriented DG films reduce from the $Ia\overline{3}d$ space group in the bulk to the rectangular p2gg plane group. Thus, these films may distort along the directions of the a and b lattice basis vectors, which point along the bulk [100] and [010] directions, but the angle γ is fixed at 90° by the symmetry of the film. (211)-oriented films exhibit even lower symmetry in the rectangular pg plane group, losing all symmetry operations from the bulk except a single glide plane. As this plane group is also rectangular, distortions along a and b are allowed, but γ is fixed at 90°. (111)-oriented films are in the hexagonal p3 plane group, in which a = b and $y = 120^{\circ}$. Therefore, the only in-plane distortion permitted is uniform swelling or shrinking relative to the bulk. (110)-oriented films are in the oblique p2 space group, meaning that a, b, and y are all allowed to vary independently. Top-down views of films in these four orientations are shown in Fig. S9, showing the unit cell shape and the allowed directions of distortion, along

with the bulk lattice directions that correspond to each edge of the unit cell.

Having identified the directions along which the films are allowed to distort, we are still left with the question of whether a given film will indeed distort along these directions and, if so, how significant the distortions will be. This requires us to know which in-plane distortions would stabilize each of the two termination planes and also depends on the film thickness. To identify the preferred in-plane distortions for a given termination plane, we can consider films with identical termination planes and identical wetting behavior at both boundaries. For such films, the distortions observed for the entire unit cell will be equivalent to the preferred distortions for this termination plane individually. However, the termination planes must be chosen carefully to make sure that their distortions align. Until this point, we have described two planes as being equivalent termination planes if they simply have the same morphologies. This is not a sufficient condition for the distortions to be aligned though, because the two boundaries could be rotated or mirrored in-plane relative to one another, causing the preferred distortions at the two boundaries to point in different directions. To ensure that the two termination planes have distortions that are perfectly aligned, we choose termination planes that are related by an inversion center on the midplane of the film. If a given termination plane prefers to distort a certain lattice parameter, then its inversion will also prefer this same distortion. Conveniently, the bulk DG space group has an inversion center at the origin, so we focus here on films where the two termination planes are equidistant from the origin of the bulk unit cell. Put another way, for a film with orientation (hkl), the plane $(hkl)_0$ must be the midplane of

As an example, consider films with (110)_{5/16} termination planes. A film in the (110) orientation may distort by changing a, b, and/or y as dictated by the p2 plane group. When the $(110)_0$ plane is the midplane of the film, the inversion center upgrades the unit cell to the 3D P2/c space group, which is in the monoclinic crystal system and can still freely distort all three in-plane lattice parameters. In Fig. 7(a), we show an image of such a film. The middle of the film has been made mostly transparent so that domain patterns at the top and bottom of the film can be clearly seen. Compositions of species A and B are shown in blue and red, respectively, as indicated by the colorbars. We have also labeled the symmetry operations that lie on the film's midplane, using the symbols given in the legend. By comparing the domain patterns at the top and bottom boundaries, it can be seen that they are indeed inversions of one another. To the right of this image, we list the distortions that are observed in a, b, and γ relative to the bulk, along with a schematic that contains arrows showing the direction of the distortions. a and y both increased by about 1.8% and b shrunk by 1.5%. These are thus the distortions that are preferred by any individual (110)_{5/16} termination plane, though the magnitude of the distortions shown in Fig. 7 may be smaller than what would be preferred at the boundary because of the bulk-like region in the middle of the film.

Now, let us compare this to a different film with $(110)_{5/16}$ termination planes that does not have an inversion center on the midplane. Such a film is shown in Fig. 7(b). This film has the same termination plane on the bottom boundary as the film in Fig. 7(a) (with the origin shifted along the **b**-direction). The

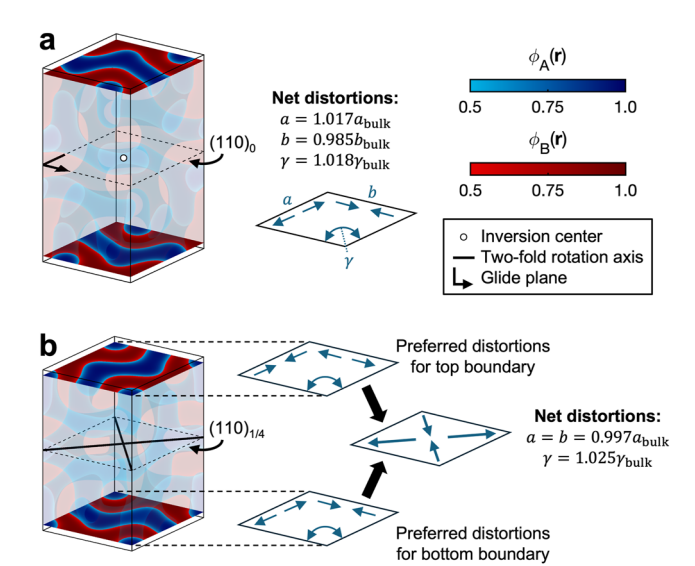


FIG. 7. In-plane distortions of (110)_{5/16}-terminated DG thin films. (a) A thin film with an inversion center. The middle of the film is made mostly transparent, while the domain patterns on the top and bottom boundaries are left fully opaque, with colors in accordance with the colorbars on the upper right. Symmetry operations are shown on the midplane, using the symbols listed in the legend. The net distortions are listed next to the image, along with a schematic showing these distortions as arrows. (b) A slightly thinner film than that in (a), which does not have an inversion center. Symmetry operations are shown on the midplane of the film. The preferred distortions at each boundary are drawn schematically, and the net distortions of the film are shown on the right.

termination plane on the top boundary is the $(110)_{5/16}$ plane located immediately below the termination plane at the top boundary in Fig. 7(a), so this film is thinner by $0.5d_{110}$. Note that the shapes of the A and B domains in the DG phase are identical for all $(110)_{5/16}$ planes, but the upper termination plane in Fig. 7(b) is a mirrorimage of the upper termination plane in Fig. 7(a). In this film, the midplane is $(110)_{1/4}$, which contains two perpendicular twofold rotation axes in the bulk, drawn on the midplane in Fig. 7(b). In the thin film, these rotation axes relate the top boundary to the bottom.

Because the top termination plane in Fig. 7(b) is aligned differently than that in Fig. 7(a), the preferred distortions are aligned differently as well. Using the distortions shown in Fig. 7(a) as a guide, we draw the preferred distortions at the top and bottom boundary separately in Fig. 7(b), revealing that the preferred distortions in a and b at the top boundary are in conflict with those preferred at the bottom boundary. The net distortion observed in the film is shown on the right in Fig. 7(b), revealing that the preferred distortions in a and b effectively cancel each other out, and the primary distortion is in y. It turns out that (110)-oriented films without an inversion center have slightly higher excess free energies than those with inversion centers [visible in Fig. S4(a)], which is a result of these aligned/unaligned distortions, though the energetic effect is so small that it is almost negligible.

The net distortions observed in the film shown in Fig. 7(b) can also be predicted from the unit cell's 3D symmetry. With the

two twofold rotation axes on the midplane, the p2 plane-group symmetry is upgraded to C222 space-group symmetry. C222 is in the orthorhombic crystal system; the unit cell shown in Fig. 7(b) is the primitive monoclinic unit cell for the centered orthorhombic lattice, and the condition a = b must be satisfied in order for the lattice to be orthorhombic. Importantly, this means that there are only two allowed modes of in-plane distortion—rather than three—because of the higher symmetry, which is evident in the net distortions observed in Fig. 7(b). More generally, for films with symmetric boundaries, one can determine the in-plane distortions that will be expected based on the symmetry operations that relate the top boundary to the bottom boundary, as these symmetry operations determine the crystal system of the thin-film unit cell, and these operations are dependent on which bulk plane is the midplane of the film.

Of course, perfectly symmetric interfaces are quite uncommon experimentally, not least because one interface is typically a substrate while the other is air. The enhanced symmetry of the film in Fig. 7(b) is only expected to occur for films confined in a slit. However, as mentioned earlier, the wetting conditions at the boundaries of an unconfined film can be tuned using methods such as the deposition of a surface modification layer on the substrate 16,77 and application of a top coat at the polymer/air boundary. 41,78 Thus, it is quite possible for an unconfined film to have nearly symmetric boundaries, in which case the principles outlined here are still applicable. Additionally, the examples in Fig. 7 more broadly illustrate the way in which the preferred distortions at the boundaries can either align or not, affecting the net distortions that are ultimately observed. Most films will experience at least a small amount of termination-dependent in-plane distortion at very low film thicknesses.

A more comprehensive dataset depicting these distortions is provided in the supplementary material. Figures S10-S17 show the lattice parameters of the DG films in Fig. 2 as a function of film thickness for confined films of polymers with $f_A = 0.36$, along with the corresponding excess free energies. These figures show that the lattice parameters distort further from their bulk values at low film thicknesses, and certain behavior alternates with each step change in the termination plane—such as whether a = c in the (110) orientation—because the midplane alternates with each step change. One particular detail worth noting is that the (001) orientation, which has a window of stability in Fig. 5, exhibits similar behavior to the (110) orientation in its a and c lattice parameters, which are equal in some films and unequal for others, depending on the midplane. Table S2 lists the 2D plane groups and 3D space groups for DG films in each orientation as a function of the midplane and whether the boundaries are symmetric. In addition to being useful for predicting the expected in-plane distortions of a film relative to the bulk, these space groups may be useful for interpreting scattering data for DG thin films as well, because the scattering peaks can be indexed to the appropriate thin-film unit cell rather than being indexed to a distorted version of the bulk cubic unit cell.

VII. CONCLUSION

In this study, we characterized the phase behavior of blockpolymer thin films containing polymers that would form the

double-gyroid phase in the bulk. Two phase diagrams were constructed, revealing the effects of film thickness, preferential wetting, and block composition on the thin-film morphology that is thermodynamically preferred. In the absence of preferential wetting, double-gyroid films in the (211) orientation are stable over a narrow composition window at thicknesses as low as $1.2a_{\text{bulk}}$, where a_{bulk} is the bulk double-gyroid lattice parameter. A-preferential boundaries (where A is the minority block) result in stabilization of perforated lamellae, while double gyroid remains stable in films with B-preferential boundaries, though a change in the termination plane is predicted. The two termination planes stabilized by B-preferential boundaries—a (001)-oriented plane and a different (211)-oriented plane—have not been observed experimentally. Additionally, we described the idea of constructive and destructive interference, in which the distortions required to accommodate the top and bottom boundaries overlap in ways that can be either favorable or unfavorable. Such interference occurs in metastable DG thin films to a much greater extent than in other thin-film phases studied previously and can cause significant variations in the free energy. Finally, we showed that the distortions to the double-gyroid morphology that are required to accommodate a flat boundary often result in a different preferred unit-cell size in the region near the boundary, which can lead to in-plane distortions of the unit cell relative to the bulk. This occurs to a more significant extent in very thin films and depends on whether or not the preferred distortions at the top boundary are aligned with those at the bottom boundary.

These results open up several promising avenues for future research. There are many important parameters that can affect the phase behavior of these films that we did not vary in this study, including conformational asymmetry, polymer dispersity, and segregation strength χN . Results may also differ slightly if a semiflexible polymer model was used rather than the continuous Gaussian chain model employed in our calculations. It is unclear how the confinement effects described herein affect other network phases, including O^{70} , 89,90 double diamond, 91 and double primitive. 92,93 Finally, the process-dependent phenomena that can result in a kinetically trapped metastable state are still poorly understood, though these effects seem to be very important in determining the film morphology that will actually be observed in a given experiment. 94

SUPPLEMENTARY MATERIAL

The supplementary material contains a pedagogical description and derivation of the thin-film common-tangent construction; a step-by-step guide for determining the space group of a thin film; an example of the spline smoothing used to perform the common-tangent calculations; the full sets of symmetry-equivalent termination planes for each film morphology in this study; an image indicating the termination planes used for parallel-oriented cylinders; a comparison between $(110)_{1/4}$ and $(110)_{5/16}$ termination planes; an alternate version of the phase diagrams showing all data points used to construct the diagrams; a figure providing more detail about the shape of the phase boundary between PL_1 and L_{\perp} ; a figure showing why there is a slanted line in Fig. 5; a figure showing the 2D unit cells, plane groups, and allowed distortions for films in each DG orientation; a set of figures showing the lattice parameters of

confined DG thin films as a function of film thickness with each termination plane; and a table providing the plane groups and space groups of all the DG thin films in this study.

ACKNOWLEDGMENTS

We thank Mahesh Mahanthappa, Michelle Calabrese, Emily McGuinness, Jinwoo Oh, Szu-Ming Yang, and Pengyu Chen for discussions. Computational resources were provided by the Minnesota Supercomputing Institute. This work was supported by the National Science Foundation through the University of Minnesota MRSEC under Award No. DMR-2011401.

AUTHOR DECLARATIONS

Conflict of Interest

The authors have no conflicts to disclose.

Author Contributions

Benjamin R. Magruder: Conceptualization (equal); Formal analysis (lead); Investigation (lead); Methodology (lead); Software (lead); Visualization (lead); Writing – original draft (lead); Writing – review & editing (equal). Christopher J. Ellison: Conceptualization (supporting); Writing – review & editing (supporting). Kevin D. Dorfman: Conceptualization (equal); Methodology (supporting); Supervision (lead); Writing – review & editing (equal).

DATA AVAILABILITY

All data in this study were generated using the open-source PSCF software (C++ version), available at https://github.com/dmorse/pscfpp. The input files, output summary files, and select output field files are available in the Data Repository for the University of Minnesota at https://hdl.handle.net/11299/264602.

REFERENCES

- ¹F. S. Bates and G. H. Fredrickson, "Block copolymers—Designer soft materials," Phys. Today **52**(2), 32–38 (1999).
- ²F. S. Bates, M. A. Hillmyer, T. P. Lodge, C. M. Bates, K. T. Delaney, and G. H. Fredrickson, "Multiblock polymers: Panacea or pandora's box?," Science 336, 434–440 (2012).
- ³C. M. Bates and F. S. Bates, "50th anniversary perspective: Block polymers—Pure potential," Macromolecules 50, 3–22 (2017).
- ⁴B. R. Magruder, D. C. Morse, C. J. Ellison, and K. D. Dorfman, "Boundary frustration in double-gyroid thin films," ACS Macro Lett. 13, 382–388 (2024).
- ⁵M. W. Matsen, "Self-assembly of block copolymers in thin films," Curr. Opin. Colloid Interface Sci. 3, 40–47 (1998).
- ⁶M. J. Fasolka and A. M. Mayes, "Block copolymer thin films: Physics and applications," Annu. Rev. Mater. Res. **31**, 323–355 (2001).
- ⁷I. Hamley, "Ordering in thin films of block copolymers: Fundamentals to potential applications," Prog. Polym. Sci. **34**, 1161–1210 (2009).
- ⁸ J. N. Albert and T. H. Epps, "Self-assembly of block copolymer thin films," Mater. Today 13, 24–33 (2010).
- ⁹C. Huang, Y. Zhu, and X. Man, "Block copolymer thin films," Phys. Rep. 932, 1–36 (2021).

- ¹⁰H. P. Huinink, J. C. M. Brokken-Zijp, M. A. Van Dijk, and G. J. A. Sevink, "Asymmetric block copolymers confined in a thin film," J. Chem. Phys. 112, 2452–2462 (2000).
- ¹¹Q. Wang, P. F. Nealey, and J. J. De Pablo, "Monte Carlo simulations of asymmetric diblock copolymer thin films confined between two homogeneous surfaces," <u>Macromolecules</u> 34, 3458–3470 (2001).
- ¹² A. Knoll, A. Horvat, K. S. Lyakhova, G. Krausch, G. J. A. Sevink, A. V. Zvelindovsky, and R. Magerle, "Phase behavior in thin films of cylinder-forming block copolymers," Phys. Rev. Lett. 89, 035501 (2002).
- ¹³ J. Bang, U. Jeong, D. Y. Ryu, T. P. Russell, and C. J. Hawker, "Block copolymer nanolithography: Translation of molecular level control to nanoscale patterns," Adv. Mater. 21, 4769–4792 (2009).
- ¹⁴C. M. Bates, M. J. Maher, D. W. Janes, C. J. Ellison, and C. G. Willson, "Block copolymer lithography," Macromolecules 47, 2–12 (2014).
- ¹⁵D. Wu, F. Xu, B. Sun, R. Fu, H. He, and K. Matyjaszewski, "Design and preparation of porous polymers," Chem. Rev. 112, 3959–4015 (2012).
- ¹⁶ N. Hampu, J. R. Werber, W. Y. Chan, E. C. Feinberg, and M. A. Hillmyer, "Next-generation ultrafiltration membranes enabled by block polymers," ACS Nano 14, 16446–16471 (2020).
- ¹⁷M. Radjabian and V. Abetz, "Advanced porous polymer membranes from self-assembling block copolymers," Prog. Polym. Sci. 102, 101219 (2020).
- ¹⁸H.-Y. Hsueh, C.-T. Yao, and R.-M. Ho, "Well-ordered nanohybrids and nanoporous materials from gyroid block copolymer templates," Chem. Soc. Rev. **44**, 1974–2018 (2015).
- ¹⁹L. Wu, W. Zhang, and D. Zhang, "Engineering gyroid-structured functional materials via templates discovered in nature and in the lab," Small 11, 5004–5022 (2015).
- ²⁰E. J. W. Crossland, M. Kamperman, M. Nedelcu, C. Ducati, U. Wiesner, D. M. Smilgies, G. E. S. Toombes, M. A. Hillmyer, S. Ludwigs, U. Steiner, and H. J. Snaith, "A bicontinuous double gyroid hybrid solar cell," Nano Lett. **9**, 2807–2812 (2009).
- ²¹ V. N. Urade, T.-C. Wei, M. P. Tate, J. D. Kowalski, and H. W. Hillhouse, "Nanofabrication of double-gyroid thin films," Chem. Mater. 19, 768–777 (2007).
- ²²M. Maldovan, A. M. Urbas, N. Yufa, W. C. Carter, and E. L. Thomas, "Photonic properties of bicontinuous cubic microphases," Phys. Rev. B **65**, 165123 (2002).
- ²³ J. A. Dolan, B. D. Wilts, S. Vignolini, J. J. Baumberg, U. Steiner, and T. D. Wilkinson, "Optical properties of gyroid structured materials: From photonic crystals to metamaterials," Adv. Opt. Mater. 3, 12–32 (2015).
- ²⁴M. Stefik, S. Guldin, S. Vignolini, U. Wiesner, and U. Steiner, "Block copolymer self-assembly for nanophotonics," Chem. Soc. Rev. 44, 5076–5091 (2015).
- ²⁵ A. Alvarez-Fernandez, C. Cummins, M. Saba, U. Steiner, G. Fleury, V. Ponsinet, and S. Guldin, "Block copolymer directed metamaterials and metasurfaces for novel optical devices," Adv. Opt. Mater. 9, 2100175 (2021).
- ²⁶B. M. Cote, W. R. Lenart, C. J. Ellison, and V. E. Ferry, "Surface structure dependent circular dichroism in single and double gyroid metamaterials," Adv. Opt. Mater. 10, 2200363 (2022).
- ²⁷H.-Y. Hsueh, H.-Y. Chen, M.-S. She, C.-K. Chen, R.-M. Ho, S. Gwo, H. Hasegawa, and E. L. Thomas, "Inorganic gyroid with exceptionally low refractive index from block copolymer templating," Nano Lett. 10, 4994–5000 (2010).
- ²⁸S. Jo, T. Jun, H. I. Jeon, S. Seo, H. Kim, S. Lee, and D. Y. Ryu, "Optical reflection from unforbidden diffraction of block copolymer templated gyroid films," ACS Macro Lett. 10, 1609–1615 (2021).
- ²⁹ D. A. Hajduk, P. E. Harper, S. M. Gruner, C. C. Honeker, G. Kim, E. L. Thomas, and L. J. Fetters, "The gyroid: A new equilibrium morphology in weakly segregated diblock copolymers," Macromolecules 27, 4063–4075 (1994).
- ³⁰M. W. Matsen and M. Schick, "Stable and unstable phases of a diblock copolymer melt," Phys. Rev. Lett. **72**, 2660–2663 (1994).
- ³¹E. W. Cochran, C. J. Garcia-Cervera, and G. H. Fredrickson, "Stability of the gyroid phase in diblock copolymers at strong segregation," Macromolecules 39, 2449–2451 (2006).

- ³² A. Reddy, M. S. Dimitriyev, and G. M. Grason, "Medial packing and elastic asymmetry stabilize the double-gyroid in block copolymers," Nat. Commun. 13, 2629 (2022).
- ³³M. W. Matsen and F. S. Bates, "Origins of complex self-assembly in block copolymers," Macromolecules 29, 7641-7644 (1996).
- ³⁴ A. Reddy, X. Feng, E. L. Thomas, and G. M. Grason, "Block copolymers beneath the surface: Measuring and modeling complex morphology at the subdomain scale," Macromolecules 54, 9223-9257 (2021).
- 35 P. Chen, M. K. Mahanthappa, and K. D. Dorfman, "Stability of cubic single network phases in diblock copolymer melts," J. Polym. Sci. 60, 2543-2552 (2022). ³⁶M. S. Dimitriyev, A. Reddy, and G. M. Grason, "Medial packing, frustration, and competing network phases in strongly segregated block copolymers," Macromolecules 56, 7184-7202 (2023).
- ³⁷M.-S. She, T.-Y. Lo, and R.-M. Ho, "Controlled ordering of block copolymer gyroid thin films by solvent annealing," Macromolecules 47, 175-182
- ³⁸J. Jung, J. Lee, H.-W. Park, T. Chang, H. Sugimori, and H. Jinnai, "Epitaxial phase transition between double gyroid and cylinder phase in diblock copolymer thin film," Macromolecules 47, 8761-8767 (2014).
- ³⁹Y.-H. Wu, T.-Y. Lo, M.-S. She, and R.-M. Ho, "Morphological evolution of gyroid-forming block copolymer thin films with varying solvent evaporation rate," CS Appl. Mater. Interfaces 7, 16536–16547 (2015).
- ⁴⁰K. Aissou, M. Mumtaz, G. Portale, C. Brochon, E. Cloutet, G. Fleury, and G. Hadziioannou, "Templated sub-100-nm-thick double-gyroid structure from Si-containing block copolymer thin films," Small 13, 1603777
- ⁴¹I. H. Ryu, Y. J. Kim, Y. S. Jung, J. S. Lim, C. A. Ross, and J. G. Son, "Interfacial energy-controlled top coats for gyroid/cylinder phase transitions of polystyrene-block-polydimethylsiloxane block copolymer thin films," ACS Appl. Mater. Interfaces 9, 17427-17434 (2017).
- ⁴²S.-M. Yang, J. Oh, B. R. Magruder, H. J. Kim, K. D. Dorfman, M. K. Mahanthappa, and C. J. Ellison, "Surface relief terraces in double-gyroidforming polystyrene-block-polylactide thin films," Phys. Rev. Mater. 7, 125601 (2023).
- ⁴³B. R. Magruder and K. D. Dorfman, *Theory of Block Polymer Self-Assembly* (American Chemical Society, Washington, DC, 2024).
- 44 See https://github.com/dmorse/pscfpp for Polymer Self-Consistent Field (PSCF) Software.
- ⁴⁵A. Arora, J. Qin, D. C. Morse, K. T. Delaney, G. H. Fredrickson, F. S. Bates, and K. D. Dorfman, "Broadly accessible self-consistent field theory for block polymer materials discovery," Macromolecules 49, 4675-4690 (2016).
- 46 G. K. Cheong, A. Chawla, D. C. Morse, and K. D. Dorfman, "Open-source code for self-consistent field theory calculations of block polymer phase behavior on
- graphics processing units," Eur. Phys. J. E 43, 15 (2020).

 47 M. W. Matsen, "Thin films of block copolymer," J. Chem. Phys. 106, 7781–7791 (1997).
- ⁴⁸V. Khanna, E. W. Cochran, A. Hexemer, G. E. Stein, G. H. Fredrickson, E. J. Kramer, X. Li, J. Wang, and S. F. Hahn, "Effect of chain architecture and surface energies on the ordering behavior of lamellar and cylinder forming block copolymers," Macromolecules 39, 9346-9356 (2006).
- ⁴⁹M. W. Matsen, "The standard Gaussian model for block copolymer melts," J. Phys.: Condens. Matter 14, R21 (2001).
- 50 G. H. Fredrickson, The Equilibrium Theory of Inhomogeneous Polymers (Oxford University Press, Oxford, 2006).
- 51 D. G. Anderson, "Iterative procedures for nonlinear integral equations," J. ACM 12, 547-560 (1965).
- 52 M. W. Matsen, "Fast and accurate SCFT calculations for periodic blockcopolymer morphologies using the spectral method with Anderson mixing," Eur. Phys. J. E 30, 361 (2009).
- ⁵³ R. B. Thompson, K. O. Rasmussen, and T. Lookman, "Improved convergence in block copolymer self-consistent field theory by Anderson mixing," J. Chem. Phys. 120, 31-34 (2004).

- ⁵⁴C. A. Tyler and D. C. Morse, "Stress in self-consistent-field theory," Macromolecules 36, 8184-8188 (2003).
- 55 A. Arora, D. C. Morse, F. S. Bates, and K. D. Dorfman, "Accelerating selfconsistent field theory of block polymers in a variable unit cell," J. Chem. Phys. 146, 244902 (2017).
- 56 G. Tzeremes, K. Ø. Rasmussen, T. Lookman, and A. Saxena, "Efficient computation of the structural phase behavior of block copolymers," Phys. Rev. E 65, 041806 (2002).
- ⁵⁷A. Ranjan, J. Qin, and D. C. Morse, "Linear response and stability of ordered phases of block copolymer melts," Macromolecules 41, 942-954
- ⁵⁸D. T. Wu, G. H. Fredrickson, J.-P. Carton, A. Ajdari, and L. Leibler, "Distribution of chain ends at the surface of a polymer melt: Compensation effects and surface tension," J. Polym. Sci., Part B: Polym. Phys. 33, 2373-2389
- ⁵⁹M. W. Matsen, "Entropic surface segregation from athermal polymer blends: Polymer flexibility vs bulkiness," J. Chem. Phys. 156, 184901 (2022).
- 60 See https://github.com/kdorfmanUMN/polymer_visual for Polymer Visual Software.
- ⁶¹ W. Bai, A. F. Hannon, K. W. Gotrik, H. K. Choi, K. Aissou, G. Liontos, K. Ntetsikas, A. Alexander-Katz, A. Avgeropoulos, and C. A. Ross, "Thin film morphologies of bulk-gyroid polystyrene-block-polydimethylsiloxane under solvent vapor annealing," Macromolecules 47, 6000-6008 (2014).
- ⁶²S. Lee, L.-C. Cheng, K. R. Gadelrab, K. Ntetsikas, D. Moschovas, K. G. Yager, A. Avgeropoulos, A. Alexander-Katz, and C. A. Ross, "Double-layer morphologies from a silicon-containing ABA triblock copolymer," ACS Nano 12, 6193-6202
- 63 S. Antoine, K. Aissou, M. Mumtaz, S. Telitel, G. Pécastaings, A.-L. Wirotius, C. Brochon, E. Cloutet, G. Fleury, and G. Hadziioannou, "Core-shell double gyroid structure formed by linear ABC terpolymer thin films," Macromol. Rapid Commun. 39, 1800043 (2018).
- ⁶⁴F. Drolet and G. H. Fredrickson, "Combinatorial screening of complex block copolymer assembly with self-consistent field theory," Phys. Rev. Lett. 83, 4317-4320 (1999).
- 65 C. L. Tsai and G. H. Fredrickson, "Using particle swarm optimization and self-consistent field theory to discover globally stable morphologies of block copolymers," Macromolecules 55, 5249-5262 (2022).
- ⁶⁶P. Chen and K. D. Dorfman, "Gaming self-consistent field theory: Generative block polymer phase discovery," Proc. Natl. Acad. Sci. U. S. A. 120, e2308698120
- 67Q. Dong, Z. Xu, Q. Song, Y. Qiang, Y. Cao, and W. Li, "Automated search strategy for novel ordered structures of block copolymers," ACS Macro Lett. 13, 987-993 (2024).
- ⁶⁸C. S. Henkee, E. L. Thomas, and L. J. Fetters, "The effect of surface constraints on the ordering of block copolymer domains," J. Mater. Sci. 23, 1685–1694 (1988).
- 69 G. Coulon, T. P. Russell, V. R. Deline, and P. F. Green, "Surface-induced orientation of symmetric, diblock copolymers: A secondary ion mass-spectrometry study," Macromolecules 22, 2581-2589 (1989).
- ⁷⁰ S. H. Anastasiadis, T. P. Russell, S. K. Satija, and C. F. Majkrzak, "Neutron reflectivity studies of the surface-induced ordering of diblock copolymer films," Phys. Rev. Lett. 62, 1852-1855 (1989).
- $^{\bf 71}\,{\rm G.}$ T. Pickett, T. A. Witten, and S. R. Nagel, "Equilibrium surface orientation of lamellae," Macromolecules 26, 3194-3199 (1993).
- ⁷²J.-U. Sommer, A. Hoffmann, and A. Blumen, "Block copolymer films between neutral walls: A Monte Carlo study," J. Chem. Phys. 111, 3728-3732 (1999).
- 73 G. Szamel and M. Müller, "Thin films of asymmetric triblock copolymers: A Monte Carlo study," J. Chem. Phys. 118, 905-913 (2003).
- $^{74}\mathrm{D}.$ Meng and Q. Wang, "Hard-surface effects in polymer self-consistent field calculations," J. Chem. Phys. 126, 234902 (2007).
- ⁷⁵E. W. Edwards, M. F. Montague, H. H. Solak, C. J. Hawker, and P. F. Nealey, "Precise control over molecular dimensions of block-copolymer domains using the interfacial energy of chemically nanopatterned substrates," Adv. Mater. 16, 1315-1319 (2004).

- ⁷⁶P. Mansky, Y. Liu, E. Huang, T. P. Russell, and C. Hawker, "Controlling polymer-surface interactions with random copolymer brushes," Science 275, 1458–1460 (1997).
- ⁷⁷D. Y. Ryu, K. Shin, E. Drockenmuller, C. J. Hawker, and T. P. Russell, "A generalized approach to the modification of solid surfaces," Science 308, 236–239 (2005).
- ⁷⁸C. M. Bates, T. Seshimo, M. J. Maher, W. J. Durand, J. D. Cushen, L. M. Dean, G. Blachut, C. J. Ellison, and C. G. Willson, "Polarity-switching top coats enable orientation of sub–10-nm block copolymer domains," Science 338, 775–779 (2012).
- ⁷⁹C. Sinturel, M. Vayer, M. Morris, and M. A. Hillmyer, "Solvent vapor annealing of block polymer thin films," Macromolecules **46**, 5399–5415 (2013).
- ⁸⁰D. Posselt, J. Zhang, D.-M. Smilgies, A. V. Berezkin, I. I. Potemkin, and C. M. Papadakis, "Restructuring in block copolymer thin films: In situ GISAXS investigations during solvent vapor annealing." Prog. Polym. Sci. **66**, 80–115 (2017)
- gations during solvent vapor annealing," Prog. Polym. Sci. 66, 80–115 (2017).

 ⁸¹ D. C. Morse and G. H. Fredrickson, "Semiflexible polymers near interfaces," Phys. Rev. Lett. 73, 3235–3238 (1994).
- ⁸²Y. Gong, W. Zhang, and R. G. Larson, "Interfacial oriented precursor to secondary nucleation of alkane oligomer crystals revealed by molecular dynamic simulations," Macromolecules 55, 6311–6320 (2022).
- ⁸³T. Geisinger, M. Müller, and K. Binder, "Symmetric diblock copolymers in thin films. I. Phase stability in self-consistent field calculations and Monte Carlo simulations," J. Chem. Phys. 111, 5241–5250 (1999).
- ⁸⁴Q. Wang, Q. Yan, P. F. Nealey, and J. J. De Pablo, "Monte Carlo simulations of diblock copolymer thin films confined between two homogeneous surfaces," J. Chem. Phys. 112, 450–464 (2000).
- ⁸⁵W. Li, M. Liu, F. Qiu, and A.-C. Shi, "Phase diagram of diblock copolymers confined in thin films," J. Phys. Chem. B **117**, 5280–5288 (2013).

- ⁸⁶M. Sikka, N. Singh, A. Karim, F. S. Bates, S. K. Satija, and C. F. Majkrzak, "Entropy-driven surface segregation in block copolymer melts," Phys. Rev. Lett. 70, 307–310 (1993).
- ⁸⁷R. K. W. Spencer and M. W. Matsen, "Universality of entropic surface segregation from athermal polymer blends due to conformational asymmetry," Macromolecules 55, 1120–1126 (2022).
- ⁸⁸G. T. Pickett and A. C. Balazs, "Equilibrium orientation of confined diblock copolymer films," Macromolecules **30**, 3097–3103 (1997).
- ⁸⁹T. S. Bailey, C. M. Hardy, T. H. Epps, and F. S. Bates, "A noncubic triply periodic network morphology in poly(isoprene-*b*-styrene-*b*-ethylene oxide) triblock copolymers," Macromolecules **35**, 7007–7017 (2002).
- ⁹⁰ M. Takenaka, T. Wakada, S. Akasaka, S. Nishitsuji, K. Saijo, H. Shimizu, M. I. Kim, and H. Hasegawa, "Orthorhombic *Fddd* network in diblock copolymer melts," Macromolecules **40**, 4399–4402 (2007).
- ⁹¹C.-Y. Chu, W.-F. Lin, J.-C. Tsai, C.-S. Lai, S.-C. Lo, H.-L. Chen, and T. Hashimoto, "Order-order transition between equilibrium ordered bicontinuous nanostructures of double diamond and double gyroid in stereoregular block copolymer," Macromolecules 45, 2471–2477 (2012).
- ⁹²C.-Y. Chang, G.-M. Manesi, C.-Y. Yang, Y.-C. Hung, K.-C. Yang, P.-T. Chiu, A. Avgeropoulos, and R.-M. Ho, "Mesoscale networks and corresponding transitions from self-assembly of block copolymers," Proc. Natl. Acad. Sci. U. S. A. 118, e2022275118 (2021).
- $^{\bf 93}$ H. Lee, S. Kwon, J. Min, S.-M. Jin, J. H. Hwang, E. Lee, W. B. Lee, and M. J. Park, "Thermodynamically stable plumber's nightmare structures in block copolymers," Science 383, 70–76 (2024).
- 94 C.-Y. Chang, Y.-H. Chen, and R.-M. Ho, "Metastable network phases from controlled self-assembly of high- χ block copolymers," Phys. Rev. Mater. **8**, 030301 (2024).